Foundations of multiple black hole evolutions

Carlos O. Lousto and Yosef Zlochower

Center for Computational Relativity and Gravitation,
School of Mathematical Sciences, Rochester Institute of Technology,
78 Lomb Memorial Drive, Rochester, New York 14623
(Dated: October 29, 2018)

We present techniques for long-term, stable, and accurate evolutions of multiple-black-hole space-times using the 'moving puncture' approach with fourth- and eighth-order finite difference stencils. We use these techniques to explore configurations of three black holes in a hierarchical system consisting of a third black hole approaching a quasi-circular black-hole binary, and find that, depending on the size of the binary, the resulting encounter may lead to a prompt merger of all three black holes, production of a highly elliptical binary (with the third black hole remaining unbound), or disruption of the binary (leading to three free black holes). We also analyze the classical Burrau three-body problem using full numerical evolutions. In both cases, we find behaviors distinctly different from Newtonian predictions, which has important implications for N-body black-hole simulations. For our simulations we use approximate analytic initial data. We find that the eighth-order stencils significantly reduce the numerical errors for our choice of grid sizes, and that the approximate initial data produces the expected waveforms for black-hole binaries with modest initial separations.

I. INTRODUCTION

The recent dramatic breakthroughs in the numerical techniques to evolve black-hole-binary spacetimes [1, 2, 3] has led to rapid advancements in our understanding of black-hole physics. Notable among these advancements are developments in mathematical relativity, including systems of PDEs and gauge choices [4, 5], the exploration of the validity of the cosmic censorship conjecture [6, 7], and the application of isolated horizon formulae [8, 9, 10, 11, 12, 13]. There are many exciting new results on recoil velocities [13, 14, 15, 16, 17, 18, 19, 20, 21, 22, 23, 24, 25, 26, 27, 28, 29, 30, 31, 32, 33, 34], post-Newtonian (PN) and numerical waveform comparisons [35, 36, 37, 38], modeling of the remnant spin [6, 10, 11, 29, 39, 40, 41], new studies of eccentric black hole binaries [7, 42, 43] and producing waveforms for matched filtering [44, 45, 46, 47, 48, 49, 50]. In particular, the recent discovery of very large merger recoil kicks for black-hole binaries with spins in the orbital plane, which was originally inferred from the results in [21], then observed in [24], and determined to have a maximum value of $4000 \ \mathrm{km \, s^{-1}}$ in [26], has had a great impact in the astrophysical community, with several groups now seeking for observational traces of such high speed holes as the byproduct of galaxy collisions [32, 51].

Three-body and four-body interactions are expected to be common in globular clusters [52, 53] and in galactic cores hosting supermassive black holes (when stellar-mass-black-hole-binary systems interact with the supermassive black hole). Hierarchical triplets of supermassive black holes might also be formed in galactic nuclei undergoing sequential mergers [54, 55]. The gravitational wave emission from such systems was recently estimated using post-Newtonian techniques [56]. The recent discovery of a probable triple quasar [57] (with estimated masses of $50 \times 10^6 M_\odot$, $100 \times 10^6 M_\odot$ and $500 \times 10^6 M_\odot$ and projected separations of between 30 and 50 kpcs) indicates that hierarchical supermassive-three-black-hole systems are possible. Triple stars and black holes are much more common in globular clusters [53], and galactic disks. The closest star to the solar system, Alpha Centauri, is a triple system, as is Polaris and HD 188753.

On the theoretical side, even in the Newtonian theory of gravity, the three-body problem is much more complicated than the two body one, and is generically chaotic. In Ref. [58] we established that our numerical formalism is able to handle the evolution of three fully relativistic bodies. In this paper we continue our quest to expand our understanding of the multiple-black-hole problem by studying a sequences of black-hole-binary—third-black-hole configurations, with the third black hole intersecting the binary along the axis of rotation, to explore the influence of a third black hole on the binary dynamics. We also examine the classical Burrau three-body problem and find that the dynamics can differ dramatically from the Newtonian prediction, with important consequences for N-body black-hole simulations.

This paper is organized as follows: in Sec. II we describe the techniques used for multiple black-hole evolutions, including eighth-order techniques and approximate initial data. In Sec. III we show the results from multiple black-hole evolutions of three families of hierarchical configurations consisting of a third black hole interacting with a black-hole binary along the binary's axis of rotation, as well as the classical Burrau three-body problem. We conclude our analysis in Sec. IV where we discuss the implications of our numerical results to black-hole astrophysics and N-body simulations. We provide the techniques to generate 2PN quasi-circular orbits of our

hierarchical three-black-hole systems in Appendix A.

II. TECHNIQUES

We evolve the three-black-hole-data-sets using the LazEv [59] implementation of the 'moving puncture approach' [2, 3]. In our version of the moving puncture approach [2] we replace the BSSN [60, 61, 62] conformal exponent ϕ, which has logarithmic singularities at the punctures, with the initially C^4 field $\chi = \exp(-4\phi)$. This new variable, along with the other BSSN variables, will remain finite provided that one uses a suitable choice for the gauge. We use the Carpet [63] driver to provide a 'moving boxes' style mesh refinement. In this approach refined grids of fixed size are arranged about the coordinate centers of each hole. The Carpet code then moves these fine grids about the computational domain by following the trajectories of the three black holes. We use AHFinderDirect [64] to locate apparent horizons.

We obtain accurate, convergent waveforms and horizon parameters by evolving this system in conjunction with a modified 1+log lapse and a modified Gamma-driver shift condition [2, 65], and an initial lapse $\alpha(t = 0) = 2/(1 + \psi_{BL}^4)$ (where ψ_{BL} is the Brill-Lindquist conformal factor discussed below). The lapse and shift are evolved with $(\partial_t - \beta^i \partial_i)\alpha = -2\alpha K$, $\partial_t \beta^a = B^a$, and $\partial_t B^a = 3/4 \partial_t \tilde{\Gamma}^a - \eta B^a$. These gauge conditions require careful treatment of χ, the inverse of the three-metric conformal factor, near the puncture in order for the system to remain stable [2, 66, 67]. As was shown in Ref. [4], this choice of gauge leads to a strongly hyperbolic evolution system provided that the shift does not become too large. Unless otherwise noted, we use a standard choice of $\eta = 6/M$ for the simulations below.

A. Approximate Initial Data

We use the puncture approach [68] to compute initial data (See also [69, 70] for similar approaches). In this approach the 3-metric on the initial slice has the form $\gamma_{ab} = (\psi_{BL} + u)^4 \delta_{ab}$, where ψ_{BL} is the Brill-Lindquist conformal factor, δ_{ab} is the Euclidean metric, and u is (at least) C^2 on the punctures. The Brill-Lindquist conformal factor is given by $\psi_{BL} = 1 + \sum_{i=1}^{n} m_i/(2r_i)$, where n is the total number of 'punctures', m_i is the mass parameter of puncture i (m_i is *not* the horizon mass associated with puncture i), and r_i is the coordinate distance to puncture i. We solve for u using the approximate solutions given in Refs. [71, 72, 73, 74], with the addition of a cross-term given below. We will use the notation of [71] to write these approximate solutions. For a spinning puncture, u has the form (Eqs. (4.23),(4.26),(4.27) of [71]):

$$u_J(\ell, \mu_J) = \mathcal{J}^2 \left(u_0^J + u_2^J \mathcal{R}^2 P_2(\mu_J) \right), \tag{1}$$

where

$$40u_0^J = \ell + \ell^2 + \ell^3 - 4\ell^4 + 2\ell^5, \tag{2a}$$
$$20u_2^J = -\ell^5, \tag{2b}$$

$\vec{\mathcal{J}} = 4\vec{J}/m^2$, m is the mass parameter, $\ell = 1/(1 + \mathcal{R})$, $\mathcal{R} = 2\hat{r}/m$, $\mu_J = \hat{J} \cdot \hat{r}$, and $P_2(x) = (3x^2 - 1)/2$ is the Legendre polynomial of degree 2. For a boosted puncture, u has the form (Eqs. (4.44),(4.48),(4.49) of [71]):

$$u_P(\ell, \mu_P) = \mathcal{P}^2(u_0^P + u_2^P P_2(\mu_P)), \tag{3}$$

where

$$\frac{32}{5}u_0^P = \ell - 2\ell^2 + 2\ell^3 - \ell^4 + \frac{1}{5}\ell^5, \tag{4a}$$
$$80\mathcal{R}\, u_2^P = 15\ell + 132\ell^2 + 53\ell^3 + 96\ell^4 + 82\ell^5 + \\ 84\ell^5/\mathcal{R} + 84\ln(\ell)/\mathcal{R}^2, \tag{4b}$$

$\vec{\mathcal{P}} = 2\vec{P}/m$ and $\mu_P = \hat{P} \cdot \hat{r}$. If the puncture is both boosted and spinning then there is a cross-term

$$u_c = (\vec{\mathcal{P}} \times \vec{\mathcal{J}}) \cdot \vec{\mathcal{R}}(1 + 5\mathcal{R} + 10\mathcal{R}^2)\ell^5/80. \tag{5}$$

For a spinning boosted puncture the approximate solution has the form

$$u = u_P + u_J + u_c + \mathcal{O}(\mathcal{P}^4) + \mathcal{O}(\mathcal{J}^4) \\ + \mathcal{O}(\mathcal{P}\mathcal{J}^3) + \mathcal{O}(\mathcal{P}^2\mathcal{J}^2) + \mathcal{O}(\mathcal{P}^3\mathcal{J}), \tag{6}$$

where the error terms linear in $\mathcal{P}$ and $\mathcal{J}$ only occur when $\vec{\mathcal{P}} \times \vec{\mathcal{J}} \neq 0$. We obtain solutions for multiple punctures by superposition. The error in this approximation scales as the inverse of the distance squared between punctures.

In this approximation the total ADM mass, linear momentum, and angular momentum are given by:
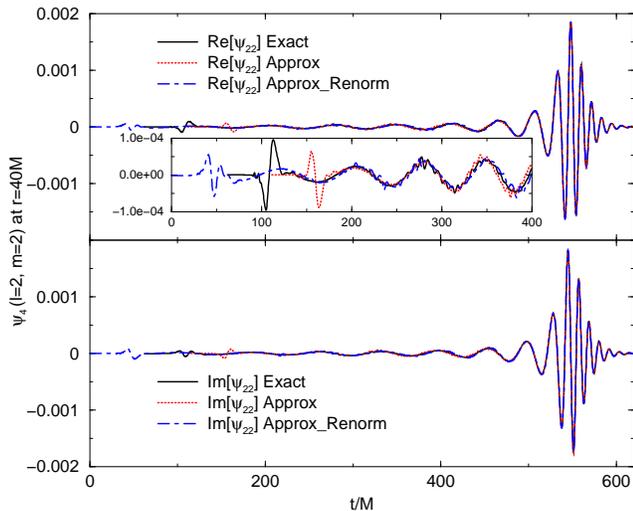
$$M_{\text{ADM}} = \sum_i m_i + \frac{2}{5}J_i^2/m_i^3 + \frac{5}{8}P_i^2/m_i, \tag{7}$$

$$\vec{P}_{\text{ADM}} = \sum_i \vec{P}_i, \tag{8}$$

$$\vec{J}_{\text{ADM}} = \sum_i (\vec{J}_i + \vec{r}_i \times \vec{P}_i). \tag{9}$$

We test the reliability of this approximate initial data by solving for equal-mass, non-spinning, quasi-circular binaries using both the TwoPunctures [75] thorn (which is restricted to problems involving two punctures) and Eq. (6). We use the 3PN equations of motion to obtain position and momentum parameters for two black holes in a binary with unit mass and a specified orbital frequency. We then choose puncture mass parameters (the same for both holes) such that the total ADM mass, as calculated using the TwoPunctures thorn, is $1M$. For our test case we choose a binary with orbital frequency $M\Omega = 0.035$ (which performs at-least three orbits prior to merger) and evolve using a relatively coarse resolution of $h = M/32$ (on the finest grid). As shown

FIG. 1: A comparison of the $(\ell = 2, m = 2)$ modes of ψ_4 at $r = 40M$ for an equal-mass, non-spinning, quasi-circular binary of mass $1M$ and orbital frequency $M\Omega = 0.035$, produced using the TWOPUNCTURES thorn (labeled 'Exact') and the approximate data (labeled 'Approx'). In both cases we used identical values for the initial data parameters (puncture mass, puncture locations, puncture momenta). The approximate data has been translated by $\delta t = 49.5M$ and multiplied by a constant phase factor of $\exp(-3.8289\,i)$. The third plot ('Approx_Renorm') shows the waveform using the approximate data with the puncture masses rescaled such that the ADM mass as given by Eq. (7) is 1M. This latter plot has been translated by $\delta t = -62M$ and multiplied by a phase factor of $\exp(4.5772\,i)$. The inset shows an expanded view of the orbital motion. Note the excellent agreement in the waveforms.

B. Eighth-Order Finite Differencing

We use both a new eighth-order spatial finite differencing algorithm and the standard fourth-order finite differencing used in our previous papers. Our eighth-order scheme extends the sixth-order scheme described in Ref. [77]. As in [77], we use a fourth-order Runge-Kutta time integrator and a second-order in time, fifth-order in space prolongation operator. Centered first spatial derivatives have the form:

$$
\begin{aligned}
\partial_x f_i &= (3f_{i-4} - 32f_{i-3} + 168f_{i-2} - 672f_{i-1} \\
&\quad - 3f_{i+4} + 32f_{i+3} - 168f_{i+2} + 672f_{i+1}) \\
&\quad /(840\,dx)
\end{aligned}
\tag{10}
$$

(we suppress the other two indices in Eqs. (10)-(13)), while for advection derivatives we adjust the center of the stencil by one point. The downward pointing stencil has the form:

$$
\begin{aligned}
\partial_x f_i &= (-3f_{i-5} + 30f_{i-4} - 140f_{i-3} + 420f_{i-2} - 1050f_{i-1} \\
&\quad + 378f_i + 420f_{i+1} - 60f_{i+2} + 5f_{i+3}) \\
&\quad /(840\,dx),
\end{aligned}
\tag{11}
$$

while the upward pointing stencil has the form:

$$
\begin{aligned}
\partial_x f_i &= (+3f_{i+5} - 30f_{i+4} + 140f_{i+3} - 420f_{i+2} + 1050f_{i+1} \\
&\quad - 378f_i - 420f_{i-1} + 60f_{i-2} - 5f_{i-3}) \\
&\quad /(840\,dx).
\end{aligned}
\tag{12}
$$

We use standard centered differencing for the second-spatial derivatives. The ∂_{xx}, ∂_{yy}, and ∂_{zz} derivatives have the form:

$$
\begin{aligned}
\partial_{xx} f_i &= \\
&(- 9f_{i-4} + 128f_{i-3} - 1008f_{i-2} + 8064f_{i-1} \\
&\quad - 9f_{i+4} + 128f_{i+3} - 1008f_{i+2} + 8064f_{i+1} \\
&\quad - 14350f_i)/(5040\,dx^2),
\end{aligned}
\tag{13}
$$

while the mixed spatial derivatives are obtained by applying Eq. (10) successively in the two direction, and have

in Fig. 1, we find that the two waveforms agree after the first half-cycle of orbital motion (we corrected for a time translation and phase difference in the waveform using the techniques of [14, 76]). The phase difference and time translation between the waveforms produced by the two methods seems to be a result of the normalization of the approximate initial data (i.e. the puncture mass parameters). When we normalize the approximate initial data such that the total approximate ADM mass (i.e. Eq. (7)) is 1M (it is only exactly 1M for the TWOPUNC-TURES data), then the binary takes longer to inspiral and the phase difference and time translation are in the opposite direction. We find, based on a linear interpolation of the phase difference and time translation versus puncture mass, that there is a puncture mass choice where both the phase difference and time translation are zero. The puncture mass that gives an ADM mass of $1M$ for the exact initial data is $m_p = 0.4891M$, the puncture mass that gives and ADM mass of $1M$ for the approximate data is $m_p = 0.4846M$, and the interpolated puncture mass that gives phase (and time) agreement between the exact and approximate waveforms is $m_p = 0.4871M$.

the form:

$$\partial_{xy} \; f_{i,j} =$$
$$\begin{aligned}
(\quad & 9f_{i-4,j-4} - 96f_{i-4,j-3} + 504f_{i-4,j-2} \\
- \quad & 2016f_{i-4,j-1} + 2016f_{i-4,j+1} - 504f_{i-4,j+2} \\
+ \quad & 96f_{i-4,j+3} - 9f_{i-4,j+4} - 96f_{i-3,j-4} \\
+ \quad & 1024f_{i-3,j-3} - 5376f_{i-3,j-2} + 21504f_{i-3,j-1} \\
- \quad & 21504f_{i-3,j+1} + 5376f_{i-3,j+2} - 1024f_{i-3,j+3} \\
+ \quad & 96f_{i-3,j+4} + 504f_{i-2,j-4} - 5376f_{i-2,j-3} \\
+ \quad & 28224f_{i-2,j-2} - 112896f_{i-2,j-1} + 112896f_{i-2,j+1} \\
- \quad & 28224f_{i-2,j+2} + 5376f_{i-2,j+3} - 504f_{i-2,j+4} \\
- \quad & 2016f_{i-1,j-4} + 21504f_{i-1,j-3} - 112896f_{i-1,j-2} \\
+ \quad & 451584f_{i-1,j-1} - 451584f_{i-1,j+1} + 112896f_{i-1,j+2} \\
- \quad & 21504f_{i-1,j+3} + 2016f_{i-1,j+4} + 2016f_{i+1,j-4} \\
- \quad & 21504f_{i+1,j-3} + 112896f_{i+1,j-2} - 451584f_{i+1,j-1} \\
+ \quad & 451584f_{i+1,j+1} - 112896f_{i+1,j+2} + 21504f_{i+1,j+3} \\
- \quad & 2016f_{i+1,j+4} - 504f_{i+2,j-4} + 5376f_{i+2,j-3} \\
- \quad & 28224f_{i+2,j-2} + 112896f_{i+2,j-1} - 112896f_{i+2,j+1} \\
+ \quad & 28224f_{i+2,j+2} - 5376f_{i+2,j+3} + 504f_{i+2,j+4} \\
+ \quad & 96f_{i+3,j-4} - 1024f_{i+3,j-3} + 5376f_{i+3,j-2} \\
- \quad & 21504f_{i+3,j-1} + 21504f_{i+3,j+1} - 5376f_{i+3,j+2} \\
+ \quad & 1024f_{i+3,j+3} - 96f_{i+3,j+4} - 9f_{i+4,j-4} \\
+ \quad & 96f_{i+4,j-3} - 504f_{i+4,j-2} + 2016f_{i+4,j-1} \\
- \quad & 2016f_{i+4,j+1} + 504f_{i+4,j+2} - 96f_{i+4,j+3} \\
+ \quad & 9f_{i+4,j+4})/(705600 \, dx \, dy). \qquad (14)
\end{aligned}$$

We modify the stencils at the refinement (and outer) boundary zones using the techniques proposed in Refs. [67, 77]. The refinement boundary points are not updated during timestep, but are updated by the prolongation operation. For the first through fourth points from the boundary, we use standard second through eighth order techniques (as described below), with the exception that we use centered derivatives for the advection terms if the up(down)winded derivatives do not fit on the grid. The first points in from the boundary are updated using standard second-order stencils, the second points using the standard fourth-order scheme (See [59]), the third points using the standard sixth-order stencils (See Ref. [77]), and the fourth points using the proposed eighth-order scheme. As in Ref. [77], we found satisfactory results using 6 buffer points. We use the standard fourth-order Kreiss-Oliger dissipation operator.

III. RESULTS

The initial data parameters for all new runs presented in this paper are given in Tables I–IV. For all of our three-black-hole runs we use a standard grid structure consisting of 11 levels of refinement with outer boundaries at $640M$ and finest resolution of $h = M/80$. All runs were performed using fourth-order techniques, except where otherwise noted.

TABLE I: Initial data parameters for configurations with a third black hole intercepting a binary along the z-axis. (x_i, y_i, z_i) and (p_i^x, p_i^y, p_i^z) are the initial position and momentum of the puncture i, m_i^p is the puncture mass parameter, m_i^H is the horizon mass, $M\Omega$ is the binary's orbital frequency, and D is the binary's initial coordinate separation. Parameters not specified are zero. Configurations are denoted by 3BHYXX, where $Y = 2, 3, 4, 5$ indicates the momentum of the third black hole, with $p_3^z = -(Y-1)P_0$ (See Eq. (15).), and XX indicates the initial binary separation.

Config	3BH203	3BH205	3BH207
y_1/M	3.6321068	5.2079414	6.9044853
z_1/M	-7.2642136	-10.415883	-13.808971
p_1^x/M	-0.0613136	-0.0483577	-0.0406335
p_1^z/M	0.0334305	0.0279183	0.0242469
m_1^p/M	0.3239234	0.3273810	0.3290810
m_1^H/M	0.3356291	0.3355032	0.3351917
y_2/M	-3.6321068	-5.2079414	-6.9044853
z_2/M	-7.2642136	-10.415883	-13.808971
p_2^x/M	-0.0613136	0.0483577	0.0406335
p_2^z/M	0.0334305	0.0279183	0.0242469
m_2^p/M	0.3239234	0.3273810	0.3290810
m_2^H/M	0.3356566	0.3355216	0.3352024
z_3/M	14.5284272	20.831766	27.617941
p_3^z/M	-0.0668610	-0.0558366	-0.0484938
m_3^p/M	0.3247293	0.3273813	0.3288641
m_3^H/M	0.3313404	0.3320131	0.3323634
$M\Omega$	0.0375000	0.0225000	0.0150000
D/M	7.2642136	10.415883	13.808971

TABLE II: continuation of Table I

Config	3BH209	3BH211	3BH303
y_1/M	8.4201027	11.117239	3.6321068
z_1/M	-16.840205	-22.234477	-7.2642136
p_1^x/M	-0.0361227	-0.0307979	-0.0613136
p_1^z/M	0.0219565	0.0191084	0.0668610
m_1^p/M	0.3299485	0.3308518	0.3171133
m_1^H/M	0.3349484	0.3346311	0.3299497
y_2/M	-8.4201027	-11.117239	-3.6321068
z_2/M	-16.840205	-22.234477	-7.2642136
p_2^x/M	0.0361227	-0.0307979	0.0613136
p_2^z/M	0.0219565	0.0191084	0.0668610
m_2^p/M	0.3299485	0.3308518	0.3171133
m_2^H/M	0.3349593	0.3346393	0.3299874
z_3/M	33.680411	44.468955	14.528427
p_3^z/M	-0.0439130	-0.0382167	-0.1337220
m_3^p/M	0.3296776	0.3305720	0.2955146
m_3^H/M	0.3255030	0.3327501	0.3075078
$M\Omega$	0.0112500	0.0075000	0.0375000
D/M	16.840205	22.234477	7.2642136

TABLE III: continuation of Table I

Config	3BH307	3BH407	3BH507
y_1/M	6.9044853	6.9044853	6.9044853
z_1/M	-13.808971	-13.808971	-13.808971
p_1^x/M	-0.0406335	-0.0406335	-0.0406335
p_1^z/M	0.0484938	0.0727407	0.0969876
m_1^p/M	0.3256512	0.3197642	0.3111199
m_1^H/M	0.3323764	0.3275486	0.3206201
y_2/M	-6.9044853	-6.9044853	-6.9044853
z_2/M	-13.808971	-13.808971	-13.808971
p_2^x/M	0.0406335	0.0406335	0.0406335
p_2^z/M	0.0484938	0.0727407	0.0969876
m_2^p/M	0.3256512	0.3197642	0.3111199
m_2^H/M	0.3324005	0.3275903	0.3205268
z_3/M	27.617941	27.617941	27.6179413
p_3^z/M	-0.0969876	-0.1454815	-0.1939753
m_3^p/M	0.3146486	0.2872890	0.2319451
m_3^H/M	0.3208728	0.2987465	0.2539505
$M\Omega$	0.0150000	0.0150000	0.0150000
D/M	13.808971	13.808971	13.808971

A. Binary—third-black-hole interactions

Initial data families of quasi-circular black-hole binaries in a hierarchical 3-body system with a third companion relatively far away from the binary were studied in Ref. [78]. That study was based on the second-order post-Newtonian (2PN) approximation to the 3-body Hamiltonian (We provide the 3-body Hamiltonian for our configurations in Appendix A.). In this work we use the 2-body Hamiltonian to generate quasi-circular black-hole binary configurations and then add a third black hole. This setup models an 'adiabatic' interaction of a binary with a third-black-hole, where the infall timescale is significantly faster than the timescale for the binary to re-circularize through the emission of gravitational radiation. Thus the binary starts off with the orbital parameters it would have if the third body were not present.

We evolve three sets of configurations with a third black hole falling towards the center of a binary perpendicular to the binary's orbital plane (which we take to be the xy plane). In all sets the third black hole is initially at a separation equal to three times the binary's separation and all black holes contribute equally to the total ADM mass given by Eq. (7) (As discussed below, they do not necessarily have similar horizon masses.). In the first set we choose the third black hole to have the momentum of a particle falling into the binary from infinity (with zero speed). We obtain this momentum by assuming that the binary separation is fixed and then treat the resulting effective two-body problem via Newtonian mechanics. We find that the third black hole has momentum

$$p_3^z = -P_0 = -\frac{4}{9}M\sqrt{\frac{M}{D\sqrt{37}}}, \qquad (15)$$

where D is the initial binary separation and M is the total mass (the binary has equal momentum in the op-

TABLE IV: Initial data parameters for the Burrau problem (3BHTR1 and 3BHTR2), as well as an off-center interaction of a binary with a third black hole falling toward the binary near the z-axis (3BHOC).

| Config	3BHOC	3BHTR1	3BHTR2
x_1/M	5.8677220	5.0000000	2.5000000
y_1/M	4.0142579	15.000000	7.5000000
z_1/M	-15.057925	0.0000000	0.0000000
p_1^x/M	-0.0206448	0.0000000	0.0000000
p_1^y/M	0.0297924	0.0000000	0.0000000
p_1^z/M	0.0232357	0.0000000	0.0000000
m_1^p/M	0.3298206	0.3000000	0.3000000
m_1^H/M	0.3355713	0.3061460	0.3122950
x_2/M	-5.8750250	-10.000000	-5.0000000
y_2/M	-4.0215595	-5.0000000	-2.5000000
z_2/M	-15.057934	0.0000000	0.0000000
p_2^x/M	0.0206502	0.0000000	0.0000000
p_2^y/M	-0.0297870	0.0000000	0.0000000
p_2^z/M	0.0232348	0.0000000	0.0000000
m_2^p/M	0.3298209	0.4000000	0.4000000
m_2^H/M	0.3355903	0.4090649	0.4181309
x_3/M	0.0073029	5.0000000	2.5000000
y_3/M	0.0073015	-5.0000000	-2.5000000
z_3/M	30.115859	0.0000000	0.0000000
p_3^x/M	-5.3366e-6	0.0000000	0.0000000
p_3^y/M	-5.3522e-6	0.0000000	0.0000000
p_3^z/M	-0.0464705	0.0000000	0.0000000
m_3^p/M	0.3292338	0.5000000	0.5000000
m_3^H/M	0.3324495	0.5104157	0.5208322
$M\Omega$	0.0150000	*********	*********
D/M	14.223576	*********	*********

posite direction). In addition, we evolve configurations with $p_3^z = -2P_0$, $p_3^z = -3P_0$, and $p_3^z = -4P_0$. We denote these configurations by 3BHYXX, where $p_3^z = -(Y-1)P_0$ and XX indicates the binary's initial separation (XX is *not* equal to the binary separation). Initial data parameters for the configurations are given in Tables I–III. In all cases the members of the binary are given linear momenta consistent with 3PN quasi-circular orbits when ignoring the contribution of the third black hole. We also evolve identical configurations of mass, initial positions, and initial momenta using a Newtonian code to compare Newtonian dynamics with the results from the fully nonlinear general relativistic evolutions. Note that the horizon mass of the third black hole is not equal to the horizon mass of the other two (the differences in the horizons masses between the members of the binary is a due solely to finite-difference errors in the isolated horizon algorithm [8]). This difference in horizon mass becomes smaller as the binary separation is increased and larger as the third-black-hole momentum is increased. It would be interesting to explore the sequence where all three black holes have the same horizon mass to see if qualitatively different results are obtained.

In Fig. 2 we show the binary separation vector $\vec{r} = \vec{r}_1 - \vec{r}_2$, projected onto the xy plane, for the first set of configurations with $p_3^z = -P_0$, as well as the Newtonian

results for these configurations (the initial third-black-hole to binary separation is three times the binary's initial separation). After rescaling by the binary's initial separation, we see that, initially, all binaries perform similar (distorted) elliptical trajectories. However, the configurations with close binary separations show a prompt triple merger of the binary and third black hole (we indicate which systems triple merge with a $*$ in the legend). As the binary's separation is increased, it undergoes more of an orbit before merging, and even receives a substantial kick from the third black hole. The plot seems to indicate that there is a critical value [42] D_{crit}, where the binary quickly merges for $D < D_{crit}$ and is given a substantial kick above this value. The Newtonian trajectories show the opposite trend, where the larger the initial binary separation, the more compact the orbit. The two systems appear to be converging to the same orbit as $\Omega \to 0$. The Newtonian orbits are scale invariant when the orbital momentum corresponds to Newtonian circular trajectories (for the two particles in the binary). As Ω is decreased and the binary separation gets large, the difference between the post-Newtonian and Newtonian momenta becomes negligible and the system becomes scale invariant. To explicitly show this, we evolved similar configurations, but with $M\Omega = 10^{-5}$ and $M\Omega = 10^{-10}$, and confirmed that the Newtonian orbit approaches the limiting trajectory given in the figure. In Fig. 3 we show the position of the third black hole versus time. Note here as well that the Newtonian and GR trends show the opposite behaviors. In the Newtonian case, the smaller D is (i.e. the larger Ω is) the more likely the third particle is to pass through the binary, while in the GR simulations the third black hole always merges with the binary for small D. The GR and Newtonian evolutions approach each other as D tends toward infinity.

In Figs. 4 and 5 we explore how the three-body system behaves when the initial z-momentum is increased, while still keeping the initial third-black-hole to binary separation at three times the binary's initial separation. We choose a relatively large initial binary separation of $D = 13.808971M = 20.7134565M_B$ (M_B is the binary's mass). In the absence of the third black hole, this binary would complete approximately 25 orbits before merging. In Newtonian theory, configurations 3BH207, 3BH407, and 3BH507 (i.e. $p_3^z = -P_0, -3P_0, -4P_0$) result in a bound binary with the third particle ejected to infinity, while for configuration 3BH307 the entire system is disrupted; leading to three free particles. Note also that in Newtonian theory the third black hole passes through the binary and is ejected toward $z = -\infty$ for all configuration except 3BH207. The GR simulations on the other hand seem to indicate that the binary is disrupted for all configuration except 2BH207 (which triple merges). Interestingly the behavior of the third particle approaches the Newtonian behavior as p_3^z is increased (as can be seen in Fig. 5). Note that, in the GR simulation of 3BH307, the third black hole was not able to escape to $z = -\infty$, but rather was bounced toward $z = +\infty$.
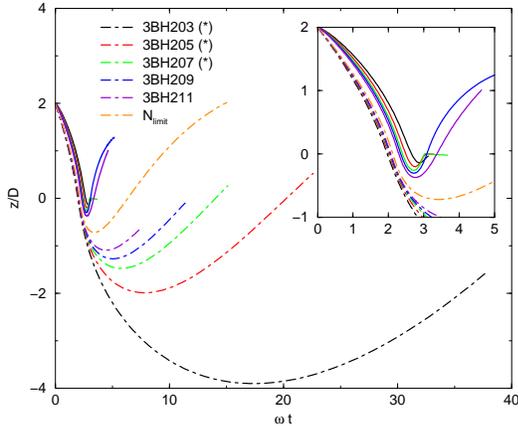
FIG. 2: The xy projection of the binary-separation trajectory when the third black hole falls towards the center of the binary along the z axis with initial momentum $p_3^z = -P_0$. The coordinates have been rescaled by the initial binary separation. The solid curves are the GR trajectories, while the dot-dashed curves are the Newtonian trajectories. N_{limit} is the Newtonian trajectory for $D \to \infty$ (i.e. $\Omega \to 0$). There seems to be a critical separation between 3BH207 and 3BH209 where the system transitions from a prompt triple merger to an elliptical binary plus third black hole (we indicate which systems triple merge with a $*$ in the legend).
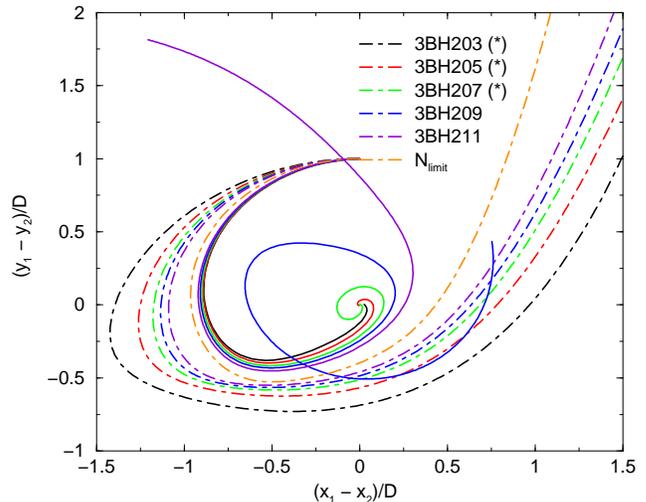
We conclude our analysis of this three-black-hole configuration by comparing the behavior of the system when the z-momentum is doubled and the binary separation is increased (while still keeping the initial third-black-hole to binary separation at three times the initial binary separation). In Fig. 6 we show the xy trajectories for configurations 3BH203, 3BH303, 3BH207, 3BH307. Note that for the closer binary (3BH203, 3BH303) increasing the momentum of the third black hole (which increases the eccentricity of the binary) causes the binary to merge sooner, while for the larger binary this same increase leads to a (possible) disruption of the binary.

It is interesting to compare the dynamics of this three-black-hole system under modified initial conditions that reduce the symmetry of the problem. We began this type of analysis by considering a purely Newtonian system consisting of a circular binary with orbital frequency $M\Omega = 0.015$ and mass $M_B = 2/3M$ (similar to 3BHY07, but with Newtonian, rather than post-Newtonian, orbital momenta) and a third particle of mass $1/3M$ located at $(x, y, z)/D = (0.0099, 0.0099, 1000)$. We then evolved this configuration using purely Newtonian evolution until the third-particle—binary separation was $\sim 3D$. We then took the Newtonian position and momentum parameters and evolved them using full GR. In the purely Newtonian evolution, this 3-body system leads to an exchange of partners in the binary, where particle 2 is ejected from the system and particles 1 and 3 form a
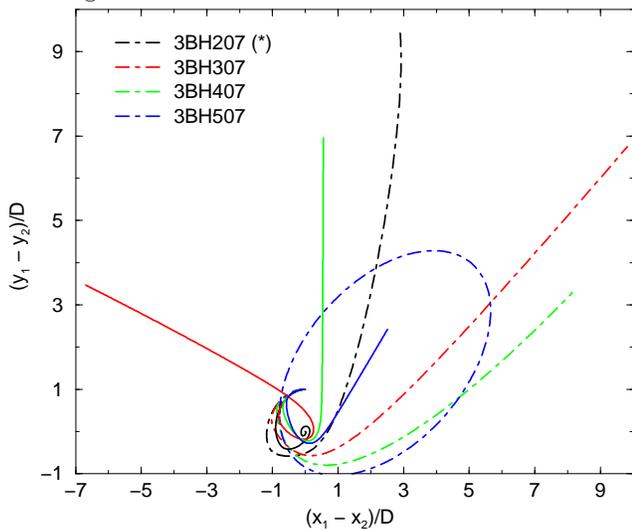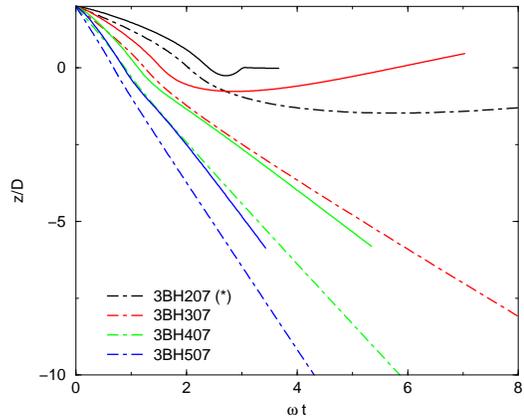
FIG. 3: The z-component (rescaled by the initial binary separation) of the trajectory of the third black hole with initial momentum $p_3^z = -P_0$. Ω is the binary's initial frequency. The solid curves are the GR trajectories, while the dot-dashed curves are the Newtonian trajectories. N_{limit} is the Newtonian trajectory for $D \to \infty$ (i.e. $\Omega \to 0$). Systems that triple-merge are indicated by a $*$ in the legend.

FIG. 5: The z-component (rescaled by the binary initial separation) of the trajectory of the third black hole with initial momentum $p_3^z = -P_0, -2P_0, -3P_0, -4P_0$. Ω is the binary's initial frequency. The solid curves are the GR trajectories, while the dot-dashed curves are the Newtonian trajectories. Systems that triple-merge are indicated by a $*$ in the legend.


FIG. 4: The xy projection of the binary-separation trajectory when the third black hole falls towards the center of the binary along the z axis with initial momentum $p_3^z = -P_0, -2P_0, -3P_0, -4P_0$. The coordinates have been rescaled by the initial binary separation. The solid curves are the GR trajectories, while the dot-dashed curves are the Newtonian trajectories. Note that 3BH207 and 3BH507 result in bound binaries in Newtonian theory. There appears to be a critical momentum where the system transitions from a prompt merger to a highly-elliptical, or perhaps even hyperbolic, orbit. Systems that triple-merge are indicated by a $*$ in the legend.

FIG. 6: The xy projection of the binary-separation trajectory when the third black hole falls towards the center of the binary along the z axis with initial momentum $p_3^z = -P_0, -2P_0$ at two different initial binary separations. The coordinates have been rescaled by the initial binary separation. Here the critical separation between prompt-merger and (possible) disruption is a function of both the binary separation and the initial z-momentum. Systems that triple-merge are indicated by a $*$ in the legend.
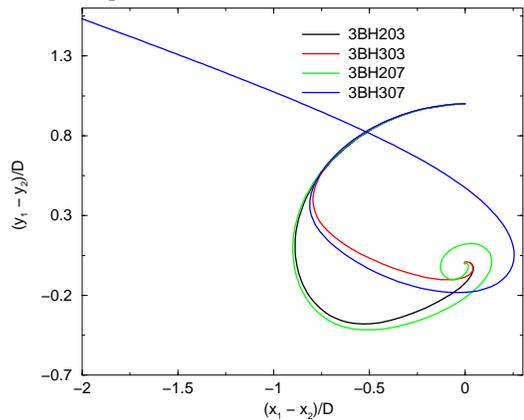
new binary with eccentricity $e = 0.645132$ (See Fig. 7). The full GR simulations, on the other hand, show a triple merger that merges faster than 3BH207 (which likely due to our using Newtonian, rather than post-Newtonian, orbital momenta). In Fig. 8 we show the xy projection of the initial binary trajectory for 3BHOC, as well as 3BH207 and the Newtonian trajectory.

FIG. 7: The xy projection of the Newtonian trajectories for 3BHOC. The initial positions of the three particles are indicated by filled circles. Note that the initial P1–P2 binary is disrupted and a new P1–P3 binary is formed (The new P1–P3 binary is inclined with respect to the xy plane.). The initial motion of P3 is essentially along the z-axis and is thus not apparent.
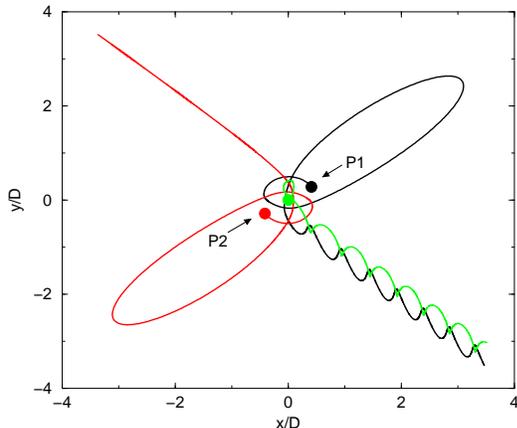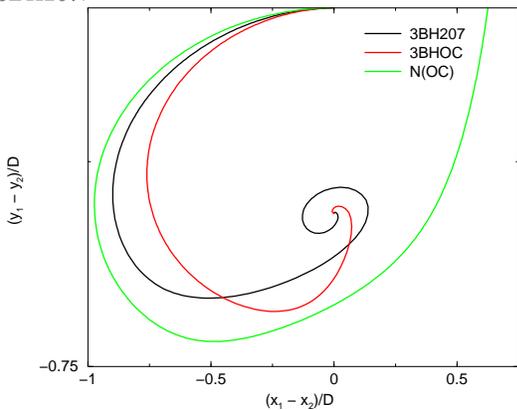
FIG. 9: The full Newtonian tracks for the 3BHTR1 configurations (3BHTR2 is obtained by rescaling by a factor of 1/2). Note that particle 1 is ejected and moves towards the upper right of the figure, while particles 2 and 3 form an elliptical binary that moves towards the lower left. Initial positions are indicated by a filled circles. Particle 1 (mass $0.3M$) is the one on top, particle 2 (mass $0.4M$) is the lower left, and particle 3 (mass $0.5M$) is the lower right. The arrows indicate the trajectories of the recoiled binary and lone particle.

FIG. 8: The xy projection of the binary-separation trajectory for 3BHOC, as well as 3BH207 and the Newtonian trajectory. Note that 3BHOC is more elliptical (and thus merges sooner) than 3BH207.
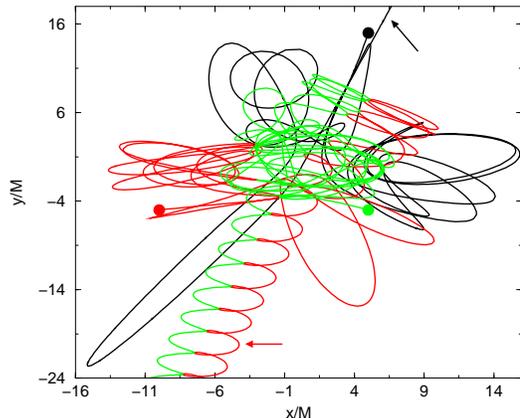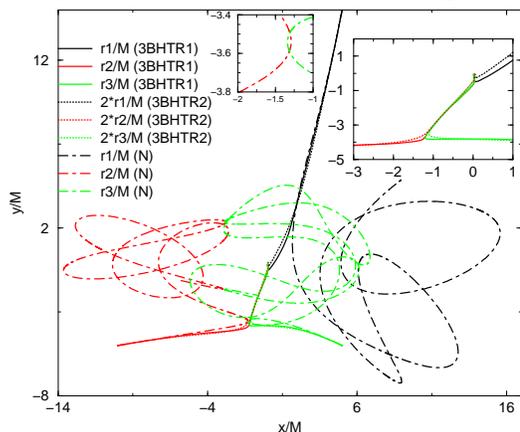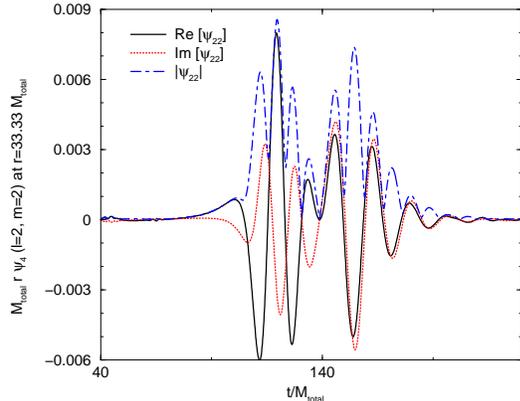
FIG. 10: The GR and Newtonian tracks for configurations 3BHTR1 and 3BHTR2, the latter rescaled by a factor of 2 (the Newtonian trajectories for these configurations are identical up to a scaling). After rescaling, the two GR trajectories are very similar (see right inset), and differ significantly from the Newtonian trajectories after the first BH2—BH3 close encounter (see left inset), which leads to a merger in GR.

B. Burrau Three-Body Configuration

Configurations 3BHTR1 and 3BHTR2 belong to a set of configurations known as the Burrau three-body problem [79, 80, 81]. This system consists of three particle, initially at rest, arranged at the vertices of a right triangle with sides of length 3ρ, 4ρ, 5ρ and masses 3μ, 4μ, 5μ, where the particle of mass $i\,\mu$ is located on the vertex opposite the side of length $i\,\rho$. After suitable rescaling, the Newtonian trajectories are independent of ρ and μ. In Newtonian theory, this configuration will lead to particles 2 and 3 forming a highly elliptical binary (with ellipticity $e \approx 0.989$), and particle 1 and the 2–3 binary ejected

in opposite directions (See Fig. 9). The trajectories of the corresponding black holes in a full GR simulation are quite different (although, if μ is kept fixed and ρ is increases, eventually the GR simulations will reproduce the Newtonian trajectories). Here we see that the trajectories scale reasonably well with ρ (i.e. compare 3BHTR1 and 3BHTR2 in Fig. 10), but rather than forming a binary and free particle, this system quickly merges to form a single black hole.

FIG. 11: The $(\ell = 2, m = 2)$ mode of ψ_4 for 3BHTR1 showing both the two mergers. Note that the imaginary part of this mode is more sensitive to the second merger. The two mergers are clearly seen in the absolute value of ψ_4.

FIG. 12: The $(\ell = 2, m = 2)$ mode of ψ_4 for 3BHTR2. Here the real part of ψ_4 seems to only indicate the presence of one merger, while the second merger is more clearly visible in the imaginary part.

The Newtonian, and even 2PN, trajectories for this three-black-hole problem will not agree with the GR trajectories if the closest approach of any two BHs is within about ten times the combined mass of the two BHs. To analyze the behavior of the system at different scales, we set the masses of the three holes to $3m$, $4m$, $5m$, and set the initial separations to $r_{13} = 200m\rho$, $r_{23} = 150m\rho$, $r_{12} = 250m\rho$. The initial merger of BH2 and BH3 seen in the GR simulation corresponds to a close approach of $r_{23}/(m_2 + m_3) = 0.054\rho$. Thus, for the initial close encounter not to lead a quick merger, we need $\rho \sim 185$, which means that the initial value of r_{23} will need to be larger than $r_{23} = 1.4 \times 10^{-9} pc(m/M_\odot)$. However, the closest approach over the entire trajectory is $r_{12}/(m_2 + m_3) = 0.0023\rho$, and in order for this approach not to lead to a prompt merger the initial value of r_{23} would need to be $r_{23} = 3.3 \times 10^{-8} pc(m/M_\odot)$.

The waveforms from 3BHTR1 and 3BHTR2 show double mergers, with the two mergers more closely spaced in 3BHTR2. In Figs. 11 and 12 we show the $(\ell = 2, m = 2)$ mode of ψ_4 extracted at $r = 40M = 33.33M_{ADM}$ (here $M_{ADM} = 1.2M$). Interestingly, the real part of the $(\ell = 2, m = 2)$ mode is more sensitive to the initial merger (of BHs 2 and 3), while the imaginary part is more sensitive to the second merger (of the 2–3 remnant with BH 1). The radiated energy and angular momentum for configuration 3BHTR1 were $E_{rad}/M_{ADM} = (8.5 \pm 1.0) \times 10^{-4}$ and $J_{rad}/M_{ADM}^2 = (2.8 \pm 2.1) \times 10^{-4}$, while for configuration 3BHTR2 the radiated quantities were $E_{rad}/M_{ADM} = (6.6 \pm 0.2) \times 10^{-4}$ and $J_{rad}/M_{ADM}^2 = (1.2 \pm 0.6) \times 10^{-4}$. The recoil velocities for 3BHTR1 and 3BHTR2 were $(4.1 \pm 2.0)\mathrm{km\,s^{-1}}$ and $(3.0 \pm 0.6)\mathrm{km\,s^{-1}}$ respectively.
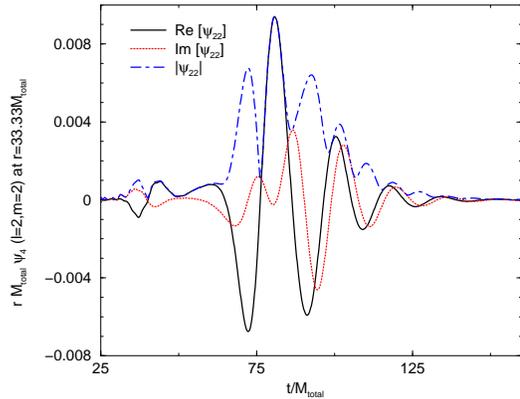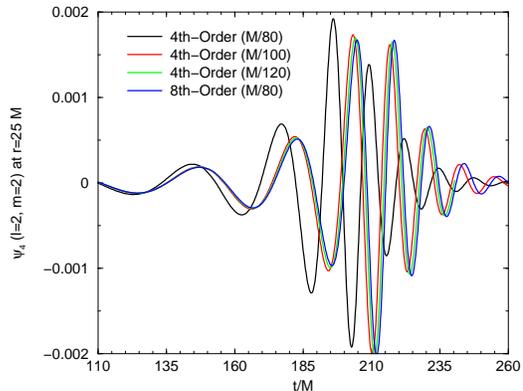
FIG. 13: The $(\ell = 2, m = 2)$ mode of ψ_4 for Q38 using both 4th and 8th-order algorithms. Note that the phase error in the $M/80$ 8th-order waveform is apparently smaller than the phase error in the $M/120$ 4th-order waveform.

C.   Eighth-Order Accuracy

We evolved several configurations, including Q38 of Refs. [13, 34] (which is a quasi-circular, non-spinning binary with mass ratio 3:8) and 3BH102 of Ref. [58] (which is a three-black-hole configuration with planar orbits), using our standard fourth-order code and the new eighth-order code. In all cases we used the same grid structure with a maximum resolution of $M/80$. In Fig. 13 we plot the $(\ell = 2, m = 2)$ component of ψ_4 for the Q38 configuration with a Gamma-driver parameter of $\eta = 2/M$. As pointed out in [34], this choice of η leads to a low effective resolution for our lowest resolution run (i.e. $M/80$), leading to a large phase error. The corresponding eighth-order run appears to be more accurate than the $M/120$ fourth-order run (i.e. its phase is closer to that predicted by extrapolating using the fourth-order $M/100$ and $M/120$ runs). Eighth-order also significantly

FIG. 14: The z component of the trajectory of BH1 for configuration 3BH102. This component should be zero by symmetry. The 8th-order algorithm produces an error that is 3.33 times smaller. Note that the error in the 4th-order trajectory is smaller than the central resolution of $M/80$ until $t \sim 290$.
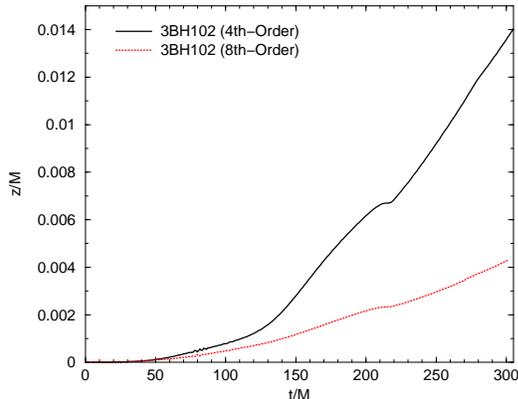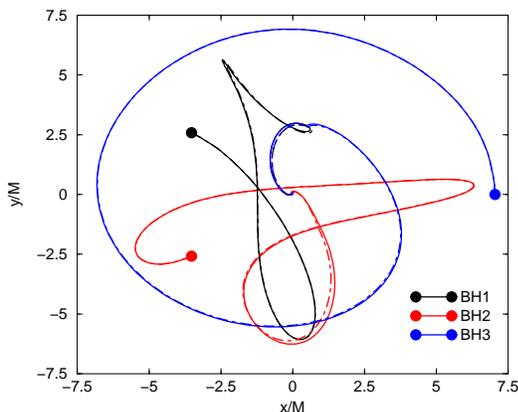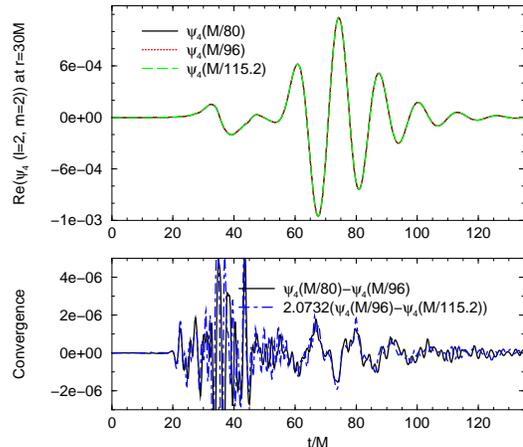

FIG. 16: The real part of the ($\ell = 2, m = 2$) mode of ψ_4 for configuration 3BH1 of Ref. [58] with central resolutions of $M/80$, $M/96$, and $M/115.2$, along with a convergence plot of data. Note the fourth-order convergence, and the smallness of the waveform amplitude.

FIG. 15: The xy projection of the trajectory of all three BHs in 3BH102. Solid curves were produced using the fourth-order algorithm; dot-dashed curved using the eighth-order algorithm.

systems using our standard algorithm.

IV. DISCUSSION

Our fully nonlinear evolutions of three-black-hole systems demonstrate dissipative General Relativistic effects due to emission of gravitational radiation and black-hole mergers, which do not have Newtonian (or even 2PN) counterparts, that dramatically change the qualitative behavior of the system. These effects become important when two objects approach each other closer than about 100 times their combined mass [82] (or $d \sim 100G(m_1 + m_2)/c^2$ in more conventional units) and become dominant when the two objects approach within about 10 times their combined mass. Even when the effect is small, the sensitivity of three (and more) body encounters to small perturbations makes including PN and GR effects important for obtaining the correct dynamics of an N-body simulation. The GR effects in particular provide a natural regularization of the Newtonian problem on small scales.

An important problem in galactic dynamics is determining how the merger process of the two (initially) central black holes proceeds after the collision of the host galaxies [83, 84, 85]. In our simulations we confirm that the resulting binary will, in general, become highly elliptical if it interacts with a similar mass black hole. These eccentric orbits will drive the binary merger due to emission of gravitational radiation. However, we also found that the interaction can produce an immediate merger of the triple system. If we set physical scale of our simulation by setting the black-hole masses to $10^9 M_\odot$, then the prompt mergers that we observe occur at separations of the order of milli-parsecs. These three-body interactions

reduces the error in three-black-hole simulations. To test this, we evolved configuration 3BH102 (which consists of three equal-mass black holes, labeled BH1 – BH3 in Fig. 15, in a planar orbit) using a shifted grid structure (i.e. one not centered on the origin) that does not exhibit the z-reflection symmetry of this configuration. In Fig. 14 we plot the z-component of the trajectory for BH1 (which should be identically zero). Note that late-time error in z is reduced by a factor of 3.33 when going from 4th to 8th-order for this coarse grid structure, which may be crucial for longer term evolutions. The xy trajectories do not change qualitatively for 3BH102 when moving to eighth-order, as is apparent in Fig. 15. We will present results from convergence and efficiency tests in a forthcoming paper. Here we note that we found fourth-order convergence (See Fig. 16) in the waveform for three-black-hole

provides a possible mechanism for resolving the "last parsec problem." [86] We will present results from the effects of unequal-masses, spins, and further separated binaries in a forthcoming paper, where we will also explore the potential for critical phenomena. It is important to note that these three-black-hole interactions provide a mechanism for producing highly-elliptical close-binaries (which would otherwise have circularized due to emission of gravitational radiation during the inspiral) like those studied in Ref. [43].

Acknowledgments

APPENDIX A: 2PN ORBITS

In this paper we did not include all Newtonian or Post-Newtonian 3-body interactions when producing initial data for quasi-circular orbits. However, these interaction can be taken into account, up to 2PN, using the Hamiltonian of the 3-body interactions in the ADM gauge as given by Eq. (5) in Ref. [87] (and Eqs. (1),(2),(A1) in Ref. [82]).

Our configurations are characterized by

$$m_1 = m_2 = m_3 = m \tag{A1a}$$
$$x_1 = 0, y_1 = r/2, z_1 = -r \tag{A1b}$$
$$x_2 = 0, y_2 = -r/2, z_2 = -r \tag{A1c}$$
$$x_3 = 0, y_3 = 0, z_3 = 2r \tag{A1d}$$
$$p_1^x = -J/r, p_1^y = 0, p_1^z = -p_3^z/2 \tag{A1e}$$
$$p_2^x = J/r, p_2^y = 0, p_2^z = -p_3^z/2 \tag{A1f}$$
$$p_3^x = 0, p_3^y = 0, \tag{A1g}$$
$$p_3^z = -\frac{4}{3}m\sqrt{\frac{3m}{r\sqrt{37}}}, \tag{A1h}$$

where r is the separation of the binary, the initial third-body—binary separation is $3r$, and the initial linear momentum of the third body corresponds to the approximate momentum it would have after falling toward the binary from infinity.

The process for computing the quasi-circular orbits proceeds as follows. We first choose a value of the orbital angular momentum, J, and then compute the linear momenta of the holes as given above in Eqs. (A1). We then compute the Hamiltonian,

$$
\begin{aligned}
H = & \ (3241792 \left(19 + \sqrt{37}\right) J^6 + 21904r \left(4 \left(-1369 + 269\sqrt{37}\right) m^3 - 37 \left(19 + \sqrt{37}\right) \left(8m^2 - 3p_3^{z\,2}\right) r\right) J^4 + \\
& \ 148r^2 \left(1152 \left(90781 + 8503\sqrt{37}\right) m^6 - 8 \left(296 \left(9583 + 709\sqrt{37}\right) m^2 + \left(13801 + 19075\sqrt{37}\right) p_3^{z\,2}\right) rm^3 + \\
& \ 1369 \left(19 + \sqrt{37}\right) \left(128m^4 - 16p_3^{z\,2}m^2 + 3p_3^{z\,4}\right) r^2\right) J^2 + r^3 \left(-128 \left(9888649 + 1247443\sqrt{37}\right) m^9 + \\
& \ 9472 \left(74 \left(1079 + 125\sqrt{37}\right) m^2 + 3 \left(100109 + 6140\sqrt{37}\right) p_3^{z\,2}\right) rm^6 - 4 \left(175232 \left(851 + 113\sqrt{37}\right) m^4 + \\
& \ 592 \left(143449 + 85651\sqrt{37}\right) p_3^{z\,2}m^2 + 3 \left(26603 - 429895\sqrt{37}\right) p_3^{z\,4}\right) r^2m^3 + \\
& \ 151959 \left(19 + \sqrt{37}\right) p_3^{z\,2} \left(128m^4 - 24p_3^{z\,2}m^2 + 11p_3^{z\,4}\right) r^3\right)) / (25934336 \left(19 + \sqrt{37}\right) m^5 r^6), \tag{A2}
\end{aligned}
$$

and find the value of r that gives a local minimum (i.e. $\partial_r H = 0$) [78], which gives the value of the separation of the binary in a quasi-circular orbit. Some of the results of this process are summarized in Table V.

[1] F. Pretorius, Phys. Rev. Lett. **95**, 121101 (2005), gr-qc/0507014.
[2] M. Campanelli, C. O. Lousto, P. Marronetti, and Y. Zlochower, Phys. Rev. Lett. **96**, 111101 (2006), gr-qc/0511048.
[3] J. G. Baker, J. Centrella, D.-I. Choi, M. Koppitz, and J. van Meter, Phys. Rev. Lett. **96**, 111102 (2006), gr-qc/0511103.
[4] C. Gundlach and J. M. Martin-Garcia, Phys. Rev. **D74**, 024016 (2006), gr-qc/0604035.

TABLE V: 2PN Initial data parameters for quasi-circular orbits of binary black holes in the presence of a third black hole. All black holes have mass $m = M/3$.

J/M^2	r/M	p_3^z/M
0.30	3.01288	-0.103819
0.35	3.61132	-0.0948274
0.40	4.58254	-0.0841810
0.45	6.33147	-0.0716168
0.50	8.85247	-0.0605668
0.55	11.7723	-0.0525215
0.60	14.9633	-0.0465858
0.65	18.4081	-0.0420013
0.70	22.1080	-0.0383259
0.75	26.0665	-0.0352960
0.80	30.2863	-0.0327449
0.85	34.7695	-0.0305610
0.90	39.5177	-0.0286663
0.95	44.5321	-0.0270042
1.00	49.8134	-0.0255325

[5] J. R. van Meter, J. G. Baker, M. Koppitz, and D.-I. Choi, Phys. Rev. **D73**, 124011 (2006), gr-qc/0605030.
[6] M. Campanelli, C. O. Lousto, and Y. Zlochower, Phys. Rev. D **74**, 041501(R) (2006), gr-qc/0604012.
[7] U. Sperhake et al. (2007), arXiv:0710.3823 [gr-qc].
[8] O. Dreyer, B. Krishnan, D. Shoemaker, and E. Schnetter, Phys. Rev. **D67**, 024018 (2003), gr-qc/0206008.
[9] E. Schnetter, B. Krishnan, and F. Beyer, Phys. Rev. **D74**, 024028 (2006), gr-qc/0604015.
[10] M. Campanelli, C. O. Lousto, and Y. Zlochower, Phys. Rev. D **74**, 084023 (2006), astro-ph/0608275.
[11] M. Campanelli, C. O. Lousto, Y. Zlochower, B. Krishnan, and D. Merritt, Phys. Rev. **D75**, 064030 (2007), gr-qc/0612076.
[12] G. B. Cook and B. F. Whiting (2007), arXiv:0706.0199 [gr-qc].
[13] B. Krishnan, C. O. Lousto, and Y. Zlochower, Phys. Rev. **D76**, 081501 (2007), arXiv:0707.0876 [gr-qc].
[14] J. G. Baker et al., Astrophys. J. **653**, L93 (2006), astro-ph/0603204.
[15] C. F. Sopuerta, N. Yunes, and P. Laguna, Phys. Rev. D **74**, 124010 (2006), astro-ph/0608600.
[16] J. A. Gonzalez, U. Sperhake, B. Bruegmann, M. Hannam, and S. Husa, Phys. Rev. Lett. **98**, 091101 (2007), gr-qc/0610154.
[17] C. F. Sopuerta, N. Yunes, and P. Laguna (2006), astro-ph/0611110.
[18] F. Herrmann, I. Hinder, D. Shoemaker, and P. Laguna, AIP Conf. Proc. **873**, 89 (2006).
[19] F. Herrmann, I. Hinder, D. Shoemaker, and P. Laguna, Class. Quant. Grav. **24**, S33 (2007).
[20] F. Herrmann, I. Hinder, D. Shoemaker, P. Laguna, and R. A. Matzner (2007), gr-qc/0701143.
[21] M. Campanelli, C. O. Lousto, Y. Zlochower, and D. Merritt, Astrophys. J. **659**, L5 (2007), gr-qc/0701164.
[22] M. Koppitz et al., Phys. Rev. Lett. **99**, 041102 (2007), gr-qc/0701163.
[23] D.-I. Choi et al. (2007), gr-qc/0702016.
[24] J. A. Gonzalez, M. D. Hannam, U. Sperhake, B. Brugmann, and S. Husa, Phys. Rev. Lett. **98**, 231101 (2007), gr-qc/0702052.
[25] J. G. Baker et al., Astrophys. J. **668**, 1140 (2007), astro-ph/0702390.
[26] M. Campanelli, C. O. Lousto, Y. Zlochower, and D. Merritt, Phys. Rev. Lett. **98**, 231102 (2007), gr-qc/0702133.
[27] E. Berti et al. (2007), gr-qc/0703053.
[28] W. Tichy and P. Marronetti, Phys. Rev. **D76**, 061502 (2007), gr-qc/0703075.
[29] F. Herrmann, I. Hinder, D. M. Shoemaker, P. Laguna, and R. A. Matzner, Phys. Rev. **D76**, 084032 (2007), arXiv:0706.2541 [gr-qc].
[30] B. Brügmann, J. A. González, M. Hannam, S. Husa, and U. Sperhake (2007), arXiv:0707.0135 [gr-qc].
[31] J. D. Schnittman et al. (2007), arXiv:0707.0301 [gr-qc].
[32] K. Holley-Bockelmann, K. Gultekin, D. Shoemaker, and N. Yunes (0700), arXiv:0707.1334 [astro-ph].
[33] D. Pollney et al. (2007), arXiv:0707.2559 [gr-qc].
[34] C. O. Lousto and Y. Zlochower (2007), arXiv:0708.4048 [gr-qc].
[35] J. G. Baker, J. R. van Meter, S. T. McWilliams, J. Centrella, and B. J. Kelly, Phys. Rev. Lett. **99**, 181101 (2007), gr-qc/0612024.
[36] Y. Pan et al. (2007), arXiv:0704.1964 [gr-qc].
[37] S. Husa, M. Hannam, J. A. Gonzalez, U. Sperhake, and B. Brugmann (2007), arXiv:0706.0904 [gr-qc].
[38] M. Hannam, S. Husa, U. Sperhake, B. Brugmann, and J. A. Gonzalez (2007), arXiv:0706.1305 [gr-qc].
[39] L. Rezzolla et al. (2007), arXiv:0708.3999 [gr-qc].
[40] P. Marronetti, W. Tichy, B. Brugmann, J. Gonzalez, and U. Sperhake (2007), arXiv:0709.2160 [gr-qc].
[41] L. Rezzolla et al. (2007), arXiv:0710.3345 [gr-qc].
[42] F. Pretorius and D. Khurana, Class. Quant. Grav. **24**, S83 (2007), gr-qc/0702084.
[43] I. Hinder, B. Vaishnav, F. Herrmann, D. Shoemaker, and P. Laguna (2007), arXiv:0710.5167 [gr-qc].
[44] B. Vaishnav, D. Shoemaker, and S. Larson, AIP Conf. Proc. **873**, 125 (2006).
[45] J. G. Baker et al., Phys. Rev. **D75**, 124024 (2007), gr-qc/0612117.
[46] P. Ajith et al. (2007), arXiv:0704.3764 [gr-qc].
[47] B. Vaishnav, I. Hinder, F. Herrmann, and D. Shoemaker (2007), arXiv:0705.3829 [gr-qc].
[48] A. Buonanno et al. (0600), arXiv:0706.3732 [gr-qc].
[49] J. G. Baker et al. (2007), arXiv:0708.4202 [astro-ph].
[50] P. Ajith et al. (2007), arXiv:0710.2335 [gr-qc].
[51] E. W. Bonning, G. A. Shields, and S. Salviander (2007), arXiv:0705.4263 [astro-ph].
[52] M. C. Miller and D. P. Hamilton (2002), astro-ph/0202298.
[53] K. Gultekin, M. C. Miller, and D. P. Hamilton, AIP Conf. Proc. **686**, 135 (2003), astro-ph/0306204.
[54] J.-c. Makino and P. Hut, The Astrophysical Journal **365**, 208 (1990).
[55] M. J. Valtonen, MNRAS **278**, 186 (1996).
[56] K. Gultekin, M. Coleman Miller, and D. P. Hamilton, Astrophys. J. **640**, 156 (2006), astro-ph/0509885.
[57] S. G. Djorgovski et al. (2007), astro-ph/0701155.
[58] M. Campanelli, C. O. Lousto, and Y. Zlochower (2007), arXiv:0710.0879 [gr-qc].
[59] Y. Zlochower, J. G. Baker, M. Campanelli, and C. O. Lousto, Phys. Rev. D **72**, 024021 (2005), gr-qc/0505055.
[60] T. Nakamura, K. Oohara, and Y. Kojima, Prog. Theor. Phys. Suppl. **90**, 1 (1987).
[61] M. Shibata and T. Nakamura, Phys. Rev. D **52**, 5428 (1995).

[62] T. W. Baumgarte and S. L. Shapiro, Phys. Rev. D **59**, 024007 (1999), gr-qc/9810065.

[63] E. Schnetter, S. H. Hawley, and I. Hawke, Class. Quantum Grav. **21**, 1465 (2004), gr-qc/0310042.

[64] J. Thornburg, Class. Quantum Grav. **21**, 743 (2004), gr-qc/0306056.

[65] M. Alcubierre, B. Brügmann, P. Diener, M. Koppitz, D. Pollney, E. Seidel, and R. Takahashi, Phys. Rev. D **67**, 084023 (2003), gr-qc/0206072.

[66] M. Campanelli, C. O. Lousto, and Y. Zlochower, Phys. Rev. D **73**, 061501(R) (2006).

[67] B. Bruegmann et al. (2006), gr-qc/0610128.

[68] S. Brandt and B. Brügmann, Phys. Rev. Lett. **78**, 3606 (1997), gr-qc/9703066.

[69] R. Beig and N. O'Murchadha, Class. Quantum Grav. **11**, 419 (1994).

[70] R. Beig and N. O'Murchadha, Class. Quantum Grav. **13**, 739 (1996).

[71] P. Laguna, Phys. Rev. D **69**, 104020 (2004), gr-qc/0310073.

[72] K. A. Dennison, T. W. Baumgarte, and H. P. Pfeiffer, Phys. Rev. **D74**, 064016 (2006), gr-qc/0606037.

[73] R. J. Gleiser, C. O. Nicasio, R. H. Price, and J. Pullin, Phys. Rev. **D57**, 3401 (1998), gr-qc/9710096.

[74] R. J. Gleiser, G. Khanna, and J. Pullin, Phys. Rev. D **66**, 024035 (2002), gr-qc/9905067.

[75] M. Ansorg, B. Brügmann, and W. Tichy, Phys. Rev. D **70**, 064011 (2004), gr-qc/0404056.

[76] J. G. Baker, M. Campanelli, F. Pretorius, and Y. Zlochower, Class. Quant. Grav. **24**, S25 (2007), gr-qc/0701016.

[77] S. Husa, J. A. Gonzalez, M. Hannam, B. Brugmann, and U. Sperhake (2007), arXiv:0706.0740 [gr-qc].

[78] M. Campanelli, M. Dettwyler, M. Hannam, and C. O. Lousto, Phys. Rev. **D74**, 087503 (2006), astro-ph/0509814.

[79] C. Burrau, Astron. Nachr. **195**, 113 (1913).

[80] V. Szebehely and C. F. Peters, AJ **72**, 876 (1967).

[81] M. J. Valtonen, S. Mikkola, and H. Pietila, mnras **273**, 751 (1995).

[82] C. O. Lousto and H. Nakano (2007), arXiv:0710.5542 [gr-qc].

[83] A. Gould and H.-W. Rix, apjl **532**, L29 (2000), arXiv:astro-ph/9912111.

[84] M. Milosavljevic and D. Merritt, Astrophys. J. **563**, 34 (2001), astro-ph/0103350.

[85] Q. Yu, mnras **331**, 935 (2002), arXiv:astro-ph/0109530.

[86] M. Milosavljevic and D. Merritt, AIP Conf. Proc. **686**, 201 (2003), astro-ph/0212270.

[87] G. Schäfer, Phys. Lett. A **123**, 336 (1987).